

## **The theoretical basis for prestack migration by equivalent offset**

Gary F. Margrave, John C. Bancroft, and Hugh D. Geiger

### **ABSTRACT**

The method of prestack migration by equivalent offset (EOM) forms common scatter point (CSP) gathers for each migrated trace and then images those gathers with a migration algorithm. The major benefits are that the CSP gathers are formed by trace mappings at constant time and that trace binning can be conveniently done as the gathers are formed. Furthermore, the CSP gathers are very sensitive velocity analysis instruments. To provide a foundation in scalar wave theory, the Fourier dual algorithm to EOM, called equivalent wavenumber migration or EWM, is derived from Fourier migration theory. Both EWM and EOM are based on the algebraic combination of a double square root equation into a single square root. This result defines equivalent wavenumber or offset. EWM is found to be an exact reformulation of prestack f-k migration. The CSP gathers are shown to be formed by a Fourier mapping, at constant frequency, of the unmigrated spectrum followed by an inverse Fourier transform. The imaging expression (for each CSP gather) which results from this analysis is formally identical to post stack migration with the result retained only at zero equivalent offset. Through a numerical simulation, the impulse responses of EOM and EWM are shown to be kinematically identical. Amplitude scale factors, which are exact in the constant velocity EWM theory, are implemented approximately in variable velocity EOM.

### **INTRODUCTION**

The modern theory of seismic wavefield imaging (migration) is generally acknowledged to rest on theoretical developments from the late 1970's and early 1980's such as Stolt (1978) Schneider (1978) and Gazdag (1978). Conventional seismic data processing is usually separated into prestack and poststack processes where "stack" refers to the common midpoint (CMP) stacking technique. Though seismic data is manifestly a wavefield, wavefield imaging techniques are usually confined to the poststack realm for economic and other practical reasons in spite of the general recognition that prestack migration is theoretically preferable. This has led to the development of DMO (dip moveout) theory which enhances the conventional image by improving the input to poststack migration. Hale (1983) put DMO theory on a firm theoretical basis by deriving its relationship to the prestack migration theory formulated in Stolt (1978). Hale proved that, for constant velocity, prestack migration is fully achieved by the cascade of three imaging steps: NMO removal, DMO correction, (stack) and poststack migration. Extension of the DMO theory to non-constant velocity has proven possible for  $v(z)$  (Hale and Artley, 1993) but problematic for  $v(x,z)$ . Thus, the theory is well formulated as a "time migration" method and has been of great practical benefit to seismic exploration.

Bancroft and Geiger (1994) and Bancroft et al. (1995) introduced an alternative technique initially called common scatterpoint (CSP) migration and now called equivalent offset migration (EOM). In a companion paper (Bancroft et al. 1996), we detail the time domain implementation and illustrate the method with real data examples. The essence of the EOM technique is to bypass CMP stacking completely by forming a new kind of gather which assumes a common subsurface scatterpoint rather than a common source-receiver midpoint. In a 2-D medium with constant velocity,  $v$ , the

expression for traveltime,  $t$ , from source to receiver via a scatterpoint at depth  $z$  and  $x=0$  (figure 1) is called the double square root (DSR) equation and is written in terms of midpoint,  $x$ , and half-offset,  $h$ , as:

$$vt = \sqrt{z^2 + (x+h)^2} + \sqrt{z^2 + (x-h)^2} = 2\sqrt{z^2 + h_e^2} \quad (1)$$

This equation also defines "equivalent offset",  $h_e$ , by asserting that the DSR can be written as a single square root. In appendix A it is shown that  $h_e$  is given exactly by:

$$h_e^2 = x^2 + h^2 - \frac{4x^2h^2}{v^2t^2} \quad (2)$$

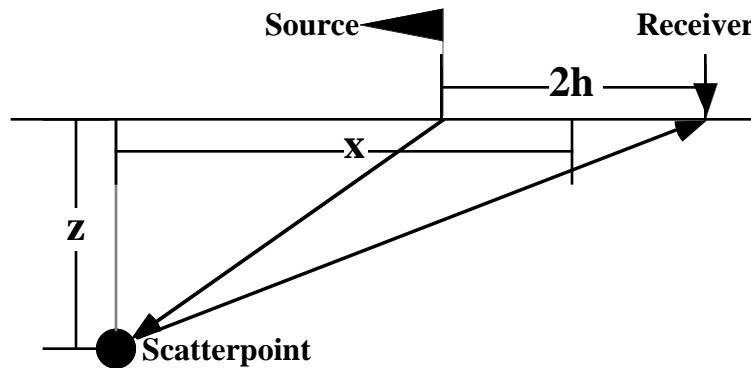


Fig. 1. The raypath geometry from source to scatterpoint and back to receiver is shown. Source and receiver are located by their midpoint,  $x$ , and half-offset,  $h$ , coordinates while the scatterpoint is at  $x = 0$  and depth  $z$ . The traveltime of scattered acoustic energy from source to receiver at constant velocity is given by equation (1).

It is well known that the traveltime surface described by (1) is not a hyperboloid in  $(x,h)$  but instead has a quasi-rectangular cross section (figure 2) and is commonly called Cheop's pyramid (Claerbout 1985). The contours in figures 2-A and 2-B were computed as constant time contours but, as equation (1) shows, they may also be considered as constant  $h_e$  contours. Using equation (2), a coordinate transformation can be defined from  $(x, h, t)$  to  $(x, h_e, t)$  which maps Cheop's pyramid into a surface with hyperbolic cross section (figures 2-C and 2-D). The triangular shape of 2-D results from requiring that  $h(x,h_e)$ , defined by solving (2) for  $h$  (see equation A-10), be a real function. Figure 2-D can then be collapsed to a hyperbola by summing all contributions at constant equivalent offset (or time). This process is repeated for all output locations to form a CSP gather at each location.

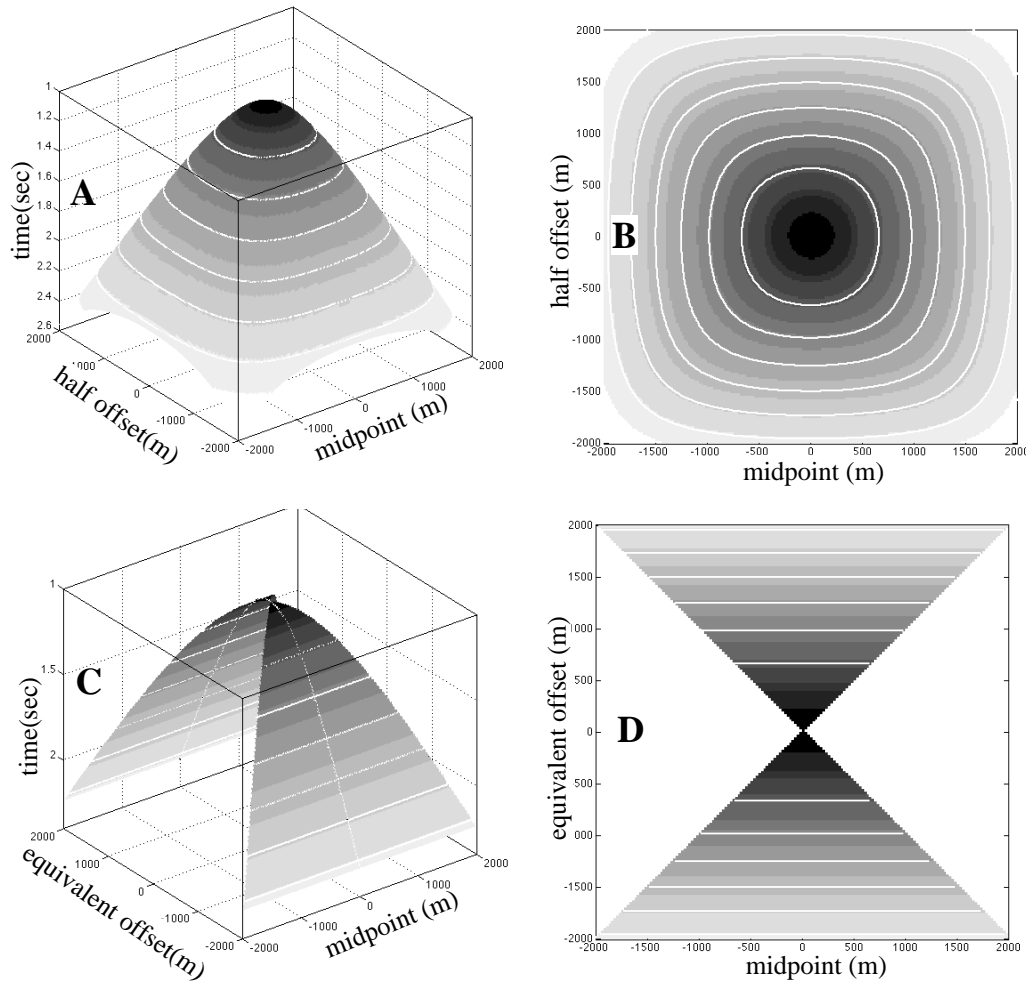


Fig. 2. A: Perspective view of Cheops pyramid (eqn 1) for a point scatterer at  $z=1000\text{m}$  with  $v=2000\text{m/sec}$ . B: Plan view of the Cheops pyramid in A. C: Perspective view of Cheops pyramid after mapping to  $(x,he,t)$  space. D: Plan view of Cheops pyramid after mapping to  $(x,he,t)$  space. Contours are constant time. The boundaries of the triangular regions (in C and D) are defined by  $\text{abs}(x) = \text{abs}(he)$ .

The impulse response of constant velocity prestack migration is an ellipse in the constant offset plane of the impulse with foci at  $x+h$  and  $x-h$ . Figure 3 shows the families of ellipses generated in two different constant offset planes through the Cheop's pyramid of figure 2-A. The bold diffraction curves in each panel are constant offset ( $h$ ) slices through Cheop's pyramid. In the zero offset case, the ellipse degenerates into a circle of radius  $t$  which replaces each point of the diffraction curve. For non-zero offset, the ellipse is shifted up by an amount equal to the NMO time shift. As is apparent in figure 3, this process focuses all offsets to the location of the scatterer.

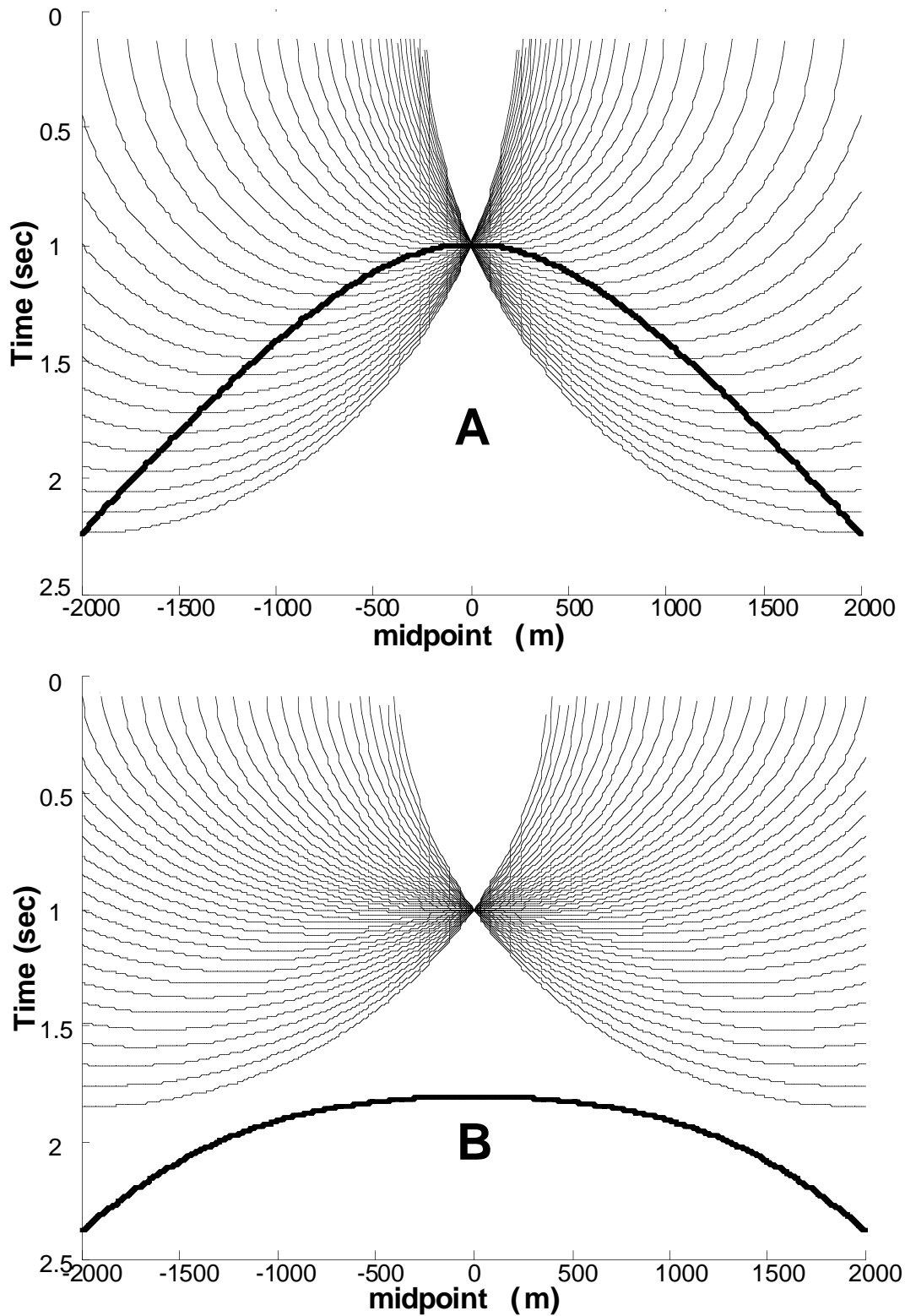


Fig. 3. An illustration of how prestack migration collapses Cheops pyramid (figure 2) to a single point. In each panel, the single bold curve is a diffraction curve (formed by slicing, at constant half-offset, through Cheops pyramid) while the family of lighter curves are ellipses of constant traveltimes. Half-offsets are 0 m (A), and 1500 m (B). The diffraction curves are migrated by replacing each point by a time shifted ellipse. The family of ellipses focus at the scatterpoint

location regardless of offset. The time shift of the ellipses is given by the NMO for a particular offset.

EOM achieves exactly the same impulse response through the numerical mechanism shown in figure 4. An impulse at  $(x_o, h_o, t_o)$  is first mapped to a hyperbola (A) in the  $t = t_o$  plane of  $(x, h_e, t)$  space. This hyperbola is  $h_e(x)$  defined by setting  $h$  and  $t$  to constants in (2) and is the contribution of the impulse to the family of CSP gathers. Then each point on the hyperbola is replaced by a wavefront circle  $h_e(t)$  (B) defined by (1). The family of wavefront circles forms the correct prestack migration ellipse (C) where they intersect the zero offset plane. (As is well known, the mechanism of point replacement by wavefront circles is equivalent to summation along constant traveltime hyperbolae.) Though this mechanism might seem complex at first, it leads to great computational savings because the formation of CSP gathers allows a convenient binning (in  $h_e$ ) and the gathers are formed by trace mappings at constant time.

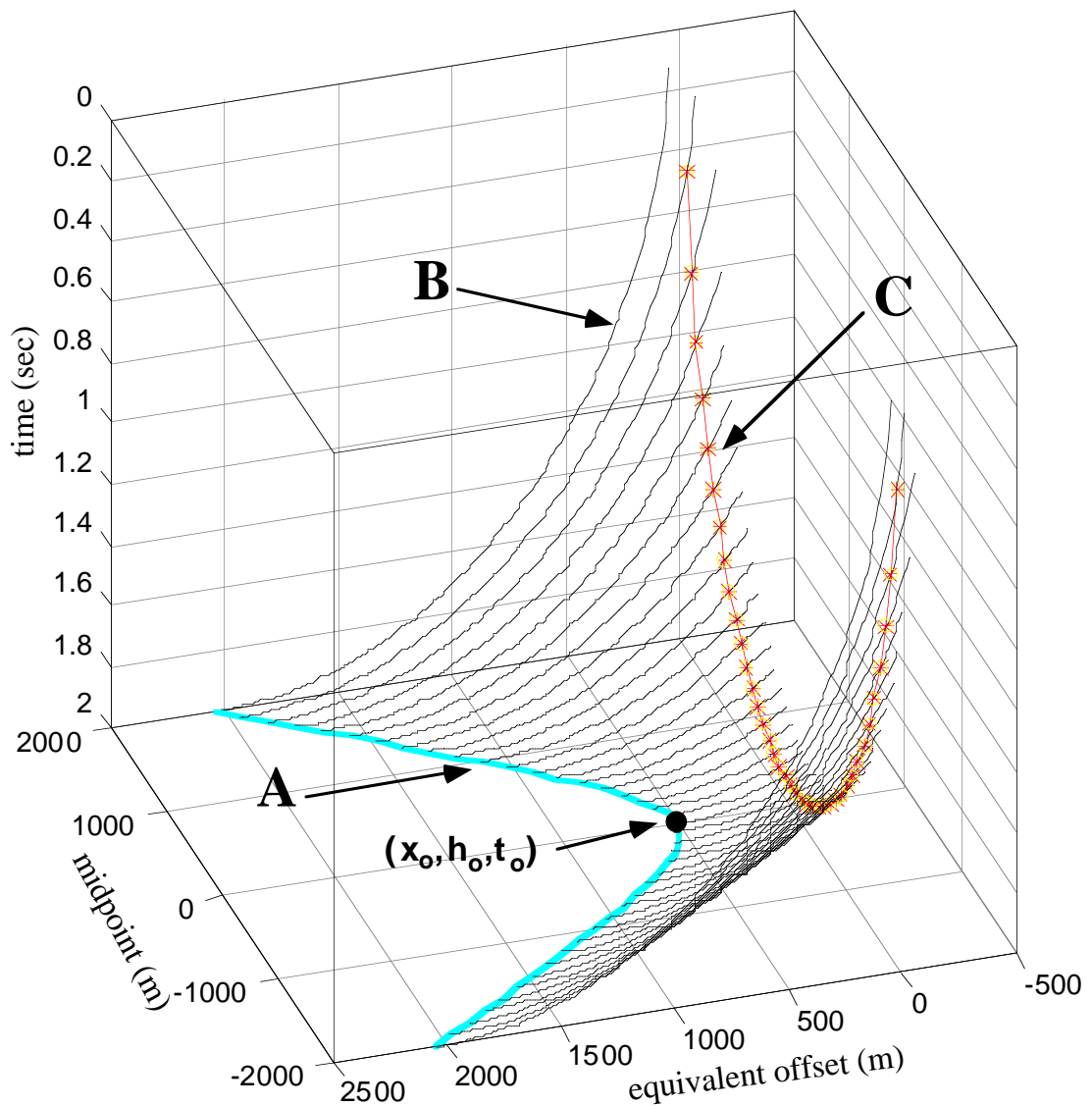


Fig. 4. The impulse response of equivalent offset migration. The input data was a single spike at inline coordinate 0, offset 500, and time 2.0. The spike is spread along the hyperbola (A) in the  $t=2.0$  plane in the process of forming CSP gathers. The migration of each CSP gather

replaces the points on the hyperbola with wavefront circles (B) in each constant  $x$  (midpoint) plane. The final image (C) is formed where the wavefront circles intersect the zero offset ( $h_e=0$ ) plane and is the ellipse predicted from constant velocity prestack migration theory.

These constant velocity concepts can easily be extended to vertical velocity variations because a vertical alignment of common scatterpoints (in  $(x,z)$ ) will result in a set of traveltimes surfaces with the same vertical alignment. Thus each CSP gather still corresponds to scattered energy from a single migrated trace. In a practical setting, migration velocities are allowed to vary from one CSP gather to another which makes the theory a "time migration".

The velocity dependence of  $h_e$  is not strong and is easily handled by the common iterative approach of assuming a trial velocity function and later refining that guess. As data is mapped into the CSP gathers, it is binned at some sensible bin size (usually half of the receiver group interval) and thus a great reduction in data volume occurs. Since the traces are mapped at constant time, no expensive trace interpolations are required (though static corrections should already be applied). Equivalent offsets are never less than source-receiver offsets (and often are much greater) so CSP gathers are much more sensitive velocity analysis instruments than CMP gathers.

Equations (1) and (2) were derived for 2-D data but similar expressions result for 3-D geometries and the equivalent offset may still be found using the generalized formalism in Appendix A. Thus, for each output point in a 3-D survey, CSP gathers may be formed in which all input traces are mapped to equivalent offset bins and scattered energy is distributed along hyperbolic paths. Conceptually, for each scatterpoint and each source-receiver pair, the vertical plane of the ray path from scatterpoint to receiver and the similar vertical plane from source to scatterpoint are rotated into a new vertical plane replicating figure 1. The variables  $x$  and  $h$  defined in the new plane facilitate the computation of the equivalent offset but do not directly relate to the original 3-D geometry.

To summarize, prestack time migration by equivalent offset is done by first forming CSP gathers for each desired migrated trace (scatterpoint position) and then imaging those gathers. Each input trace contributes to all CSP gathers within the migration aperture and is mapped at constant time to a spatial position in each gather given by the trace's equivalent offset. Once final velocities are determined (and the gathers reformed if the initial guess velocity was wildly wrong) the final imaging is done by migrating each gather with an algorithm identical to post-stack migration and evaluating (retaining) the migrations only at zero equivalent offset. Thus another large saving over conventional prestack Kirchhoff techniques is realized because the time consuming steps of dip dependent scaling and antialias filtering are performed on the CSP gathers. The first order approximation to this imaging step is conventional NMO correction and stacking of the CSP gathers.

The preceding justifications of EOM are purely kinematic. Next, we present a formal justification of EOM by showing that, in the constant velocity case, it is a Kirchhoff analog to prestack migration as formulated by Stolt (1978) in the Fourier domain. This is done by deriving, from Stolt's equations, the Fourier parallel to EOM, which we call equivalent wavenumber migration (EWM), and then showing that EOM is a conventional Kirchhoff analog to EWM while the latter is an exact prestack migration in the Fourier domain. Thus the theoretical basis for EOM is at least as good as that of NMO-DMO-poststack migration. The extension of both algorithms to the practical case of non-constant velocity is approximate though we believe there are a number of significant advantages to EOM (as mentioned above).

## DERIVATION OF THE EQUIVALENT WAVENUMBER ALGORITHM

Let  $\Psi_0(x,h,t)$  represent the prestack data for a 2-D experiment in midpoint and half-offset coordinates. Then its 3-D Fourier transform is:

$$\phi_0(k_x, k_h, \omega) = \iiint \Psi_0(x, h, t) e^{i\omega t} e^{-ik_x x} e^{-ik_h h} dx dh dt$$

or 
$$\phi_0(k_x, k_h, \omega) = \iiint \Psi_0(x, h, t) \exp(i\omega t - i k_x x - i k_h h) dx dh dt \quad (3)$$

Here  $k_x$  and  $k_h$  are wavenumbers for  $x$  and  $h$  while  $\omega$  is temporal frequency. (Note that these two expressions differ only in mathematical syntax and are both presented for clarity. Also we neglect the Fourier transform constant scale factors). Stolt's prestack theory then leads to the following expression for the "Stolt wavefield":

$$\Psi(x, h, t, z) = \iiint \phi_0(k_x, k_h, \omega) \exp(i k_z z) \exp(-i\omega t + i k_x x + i k_h h) dk_x dk_h d\omega \quad (4)$$

where:

$$k_z = \frac{1}{2} \sqrt{\left[\frac{2\omega}{v}\right]^2 - [k_x - k_h]^2} + \frac{1}{2} \sqrt{\left[\frac{2\omega}{v}\right]^2 - [k_x + k_h]^2} \quad (5)$$

Equation (4) is an explicit formula for the Stolt wavefield in terms of the prestack data. The Stolt wavefield is a four dimensional construct that can be evaluated to yield either the prestack data or the migrated section as follows:

$$\begin{aligned} \Psi(x, h, t, z=0) &= \Psi_0(x, h, t) = \iiint \phi_0(k_x, k_h, \omega) \exp(-i\omega t + i k_x x + i k_h h) dk_x dk_h d\omega \\ &= \text{the prestack data} \end{aligned} \quad (6a)$$

and

$$\begin{aligned} \Psi(x, h=0, t=0, z) &= \iiint \phi_0(k_x, k_h, \omega) \exp(i k_z z) \exp(i k_x x) dk_x dk_h d\omega \\ &= \text{the prestack migrated section} \end{aligned} \quad (6b)$$

These expressions, first derived by Stolt (1978), are presented in a variation of the notation of Hale (1983) and a summary derivation may also be found in Gazdag and Sguazzero (1984). The vertical wavenumber,  $k_z$ , as given by (5), is found from a double square root equation which is the Fourier dual of equation (1). In precisely the same way as the time domain derivation (Bancroft and Geiger 1994, Bancroft et al. 1995), the Fourier DSR can be rewritten as a single square root involving a new "equivalent" wavenumber. Thus we define equivalent wavenumber,  $k_e$ , implicitly through:

$$2k_z = \sqrt{k^2 - [k_x - k_h]^2} + \sqrt{k^2 - [k_x + k_h]^2} = 2\sqrt{k^2 - k_e^2} \quad \text{where } k = \frac{2\omega}{v} \quad (7)$$

The algebraic solution for  $k_e$  is presented in Appendix A. The result is:

$$k_e^2 = k_x^2 + k_h^2 + \frac{k_x^2 k_h^2}{k_z^2} = \frac{1}{2} [k_x^2 + k_h^2 + k^2] - \frac{1}{2} \sqrt{[k^2 - k_x^2 - k_h^2]^2 - 4k_x^2 k_h^2} \quad (8)$$

Note that (8) presents two equivalent forms for  $k_e$ , the second being better suited to our derivation but the first is more comparable to (2). Figure 5 shows  $k_z(k_x, k_h)$  in perspective view (A) and plan view (B). The diamond shaped domain of computation is defined as the range of  $(k_x, k_h)$  for which  $k_z$  is real and thus evanescent waves are not represented. Note the strong similarity to figure 2. Figures 5-C and 5-D show  $k_z(k_x, k_e)$  in perspective and plan views. Note that contours of  $k_z$  (the migration phase shift) have become functions of  $k_e$  only which suggests that great simplification can be found by mapping the prestack spectrum from  $(k_x, k_h)$  space to  $(k_x, k_e)$  space.

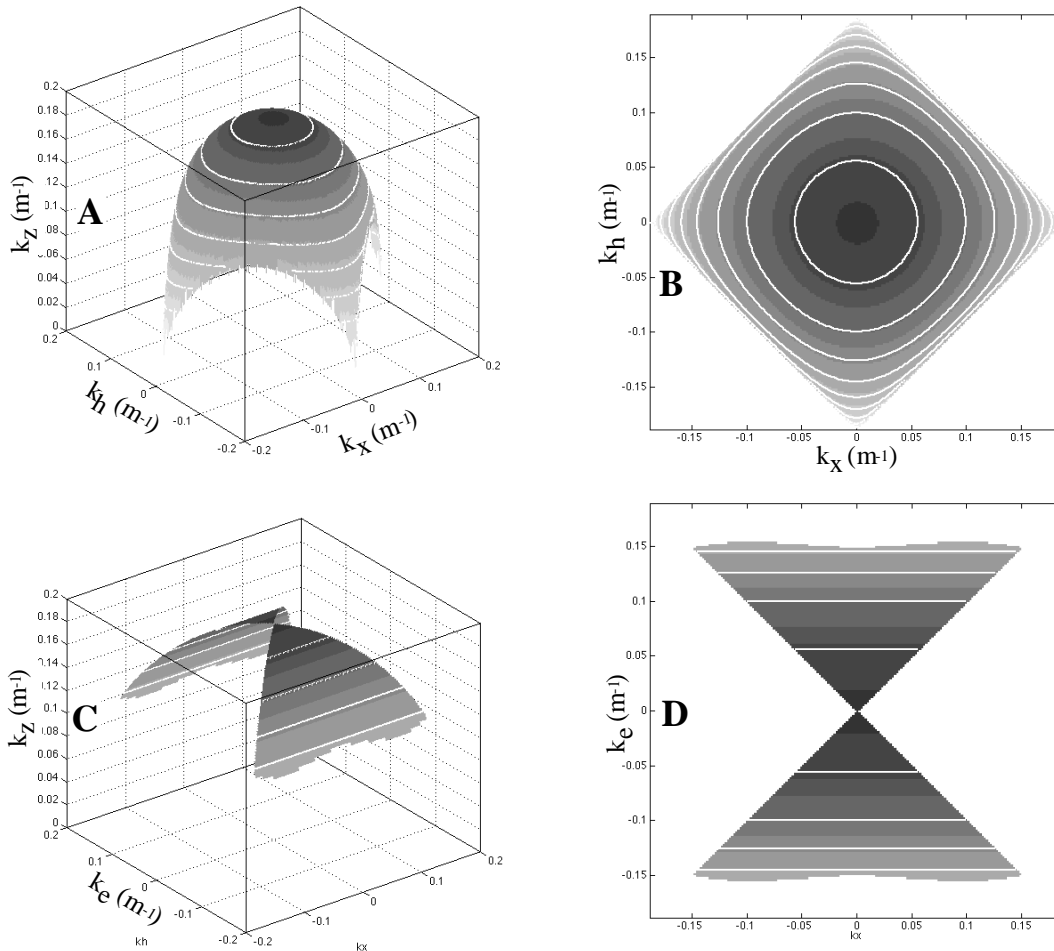


Fig. 5. A: Perspective view of the  $k_z$  surface (eqn 5) for a prestack migration with  $v=2000\text{m/sec}$  and frequency  $= (2\pi)30$ . B: Plan view of the surface in A. C: Perspective view of the  $k_z$  surface after mapping to  $(k_x, k_e, k_z)$  space. D: Plan view of the  $k_z$  surface after mapping to  $(k_x, k_e, k_z)$  space. Contours are constant  $k_z$ . The diagonal boundaries of the triangular regions (in C and D) are defined by  $\text{abs}(k_x) = \text{abs}(k_e)$ .

We proceed by changing the Fourier integration variables in (6b) from  $(k_x, k_h, k)$  to  $(k_x, k_e, k)$ . The details of the derivation are in Appendix B and the results are:

$$\Psi(x, h=0, t=0, z) = \frac{v}{2} \iint \bar{\phi}(x, k_e, k) \exp\left(i \sqrt{k^2 - k_e^2} z\right) dk_e dk \quad (9)$$

where:

$$\bar{\phi}(x, k_e, k) \equiv \int f(k_x, k_e, k) \bar{\phi}_0(k_x, k_e, k) \exp\left(ik_x x\right) dk_x \quad (10)$$

and:

$$\begin{aligned} \bar{\phi}_0(k_x, k_e, k) &= \bar{\phi}_0\left(k_x, \text{sign}(k_h) \sqrt{\frac{1}{2}[k_x^2 + k_h^2 + k^2]} - \frac{1}{2} \sqrt{[k^2 - k_x^2 - k_h^2]^2 - 4k_h^2 k_x^2}, k\right) \\ &= \phi_0(k_x, k_h, k) \end{aligned} \quad (11)$$

and:

$$f(k_x, k_e, k) = \frac{k_e}{k_h(k_e)} \left[ 1 - \frac{k_e^2 - k_h^2(k_e)}{k^2 + k_x^2 - k_e^2} \right] \text{ with } k_h(k_e) = \text{sign}(k_e) \sqrt{\frac{[k^2 - k_e^2][k_e^2 - k_x^2]}{k^2 - k_e^2 + k_x^2}} \quad (12)$$

### DISCUSSION AND EXTENSIONS

Equation (9) is an exact reformulation of (4) and thus represents a solution to the constant velocity migration problem of the same accuracy as Stolt's FK theory. While (4) involves a triple integration, a double integration is apparent in (9) because one integral has been absorbed into the definition of  $\bar{\phi}(x, k_e, k)$ . Thus, each  $x$  location is imaged independently in (9) because all  $x$  data movement has been incorporated into  $\bar{\phi}(x, k_e, k)$ .

We identify the function  $\bar{\phi}(x, k_e, k)$ , given by (10), as the Fourier transform (2D) of CSP gathers at location  $x$ . Equations (11) and (12) show that  $\bar{\phi}(x, k_e, k)$  is computed by mapping at constant temporal frequency (i.e.  $k$ ) the spectrum of the unmigrated data,  $\phi_0(k_x, k_h, k)$  from  $(k_x, k_h)$  space to  $(k_x, k_e)$  space (note that we map  $k_h$  to  $k_e$  of the same sign) and applying a scaling operation, followed by an inverse Fourier transform over  $k_x$ . Though algebraically complex, the mapping operation is conceptually simple when depicted graphically as in figure 5. Essentially, each contour in figure 5-B becomes horizontal in 5-D. Figure 5-B can be imagined split along  $k_h = 0$  with the upper half mapping to the upper triangle of 5-D and vice-versa for the lower half. The point where a given contour in 5-B touches  $k_h = 0$  maps to one of the diagonal boundaries of the triangular regions in 5-D. (These boundaries are determined by  $\text{abs}(k_e) = \text{abs}(k_x)$  and are not evanescent boundaries. The evanescent boundary is at the top (or bottom) of the triangles.) The mapping causes no spectral distortion along  $k_x = 0$  and maximal distortion at  $k_h = 0$ .

The scaling operation is simply that required to conserve the total integrated spectrum. The scale factor  $f(k_x, k_e, k)$  is a purely real function of the wavenumbers and does not have a (complex) phase term. Figure 6 examines the function  $f$  given by (12) which is the entire scaling function applied to the spectrum as it is mapped. In 6-A which shows the function  $f$  at constant values of  $kh$ , the curves end at the  $kx$  axis (at  $kh = k - kx$ ) which corresponds to the transition to evanescent energy. A curve is not shown for  $kh = 0$  because the scaling factor is infinite. Intuitively,  $kh = 0$  is expected to correspond to horizontal events in a CMP gather which occur only at zero offset; however, this is an instantaneous spectral notion. Any real Fourier spectrum over some range of offsets will always contain  $kh = 0$  as well as other spectral components and a practical implementation of this theory would have to apply a finite scale factor. Figure 6-B shows a map of  $f(k_x, k_e, k)$  over  $(kx, kh)$  space similar to 5-B. It is apparent that the scaling factors are near unity over most of the spectrum with large values occurring only near zero  $kh$  for non-zero  $kx$ .

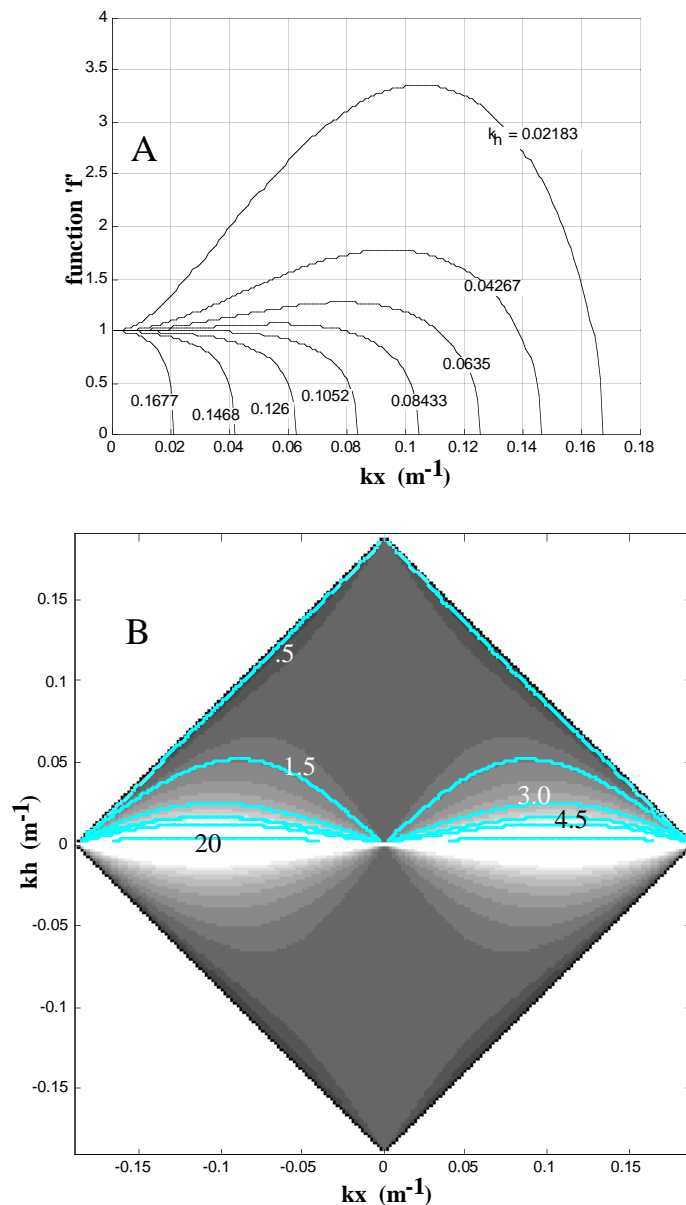


Fig. 6. A: The spectral scaling function,  $f(k_x, k_e, k)$ , is shown versus  $k_x$  for  $k = 186$  and for a range of different  $k_h(k_e)$  values. Each curve is labeled with its  $k_h$  value. The curves terminate at  $k_x = k - k_h$  which is the evanescent boundary of  $k_z(k_x, k_h)$  as shown in figure 6-B. B: The function  $f(k_x, k_e, k)$  is shown in map view. White is large amplitude and black is a value near 1. Contours are shown only on the top half of the figure for clarity.

The reason for these large scaling factors near  $k_h = 0$  is that the mapping compresses this portion of the spectrum greatly into the boundary near  $k_e = k_x$  (figure 5-D). In order to conserve the total integrated spectrum, the compressed portion of the spectrum must increase in amplitude. Put another way, if the migration is performed without these scaling factors, then the low  $k_h$  values will not contribute their proper strength to the final image. Intuitively,  $k_x = 0$  must correspond to flat events immediately beneath the scatter point. Since  $k_x = 0$  is passed undistorted,  $k_h = 0$  at  $k_x = 0$  is also unaffected. Spectral components with  $k_h = 0$  but at other values of  $k_x$  must correspond to scattered energy from some non-zero inline distance away from the scatter point. Thus these events have a finite equivalent offset and map to a position some distance down a hyperbola in the CSP gather and hence to a dipping event in  $k_e$ . Thus  $k_h = 0$  always maps to some finite  $k_e$  unless  $k_x$  also is zero.

The recognition that equation (10) forms CSP gathers in the Fourier domain stems from several observations. We have already noted that, whatever  $\bar{\phi}(x, k_e, k)$  is, it is imaged independently for each  $x$  by diffraction summation precisely as is expected of CSP gathers. Ideally, we would like to be able to show that the impulse response of (10) is essentially the constant-time hyperbola discussed previously and shown in figure 4. We have not been able to do this analytically and so present a numerical simulation in figure 7. To create this image, we constructed the analytic spectrum of an impulse at  $x = 0$ ,  $h = 500$ , and  $t = 2.0$ . This was mapped to  $(k_x, k_e)$ , scaled by  $f$ , and the inverse Fourier transforms were performed numerically. The result is shown in figure 7 for the  $t = 2.0$  plane and is kinematically identical to the hyperbola in figure 4. The additional amplitude effects are contained in the scaling described here as required by scalar wave theory.

An approximate implementation of this scaling factor in a space-time Kirchhoff algorithm can proceed by first writing:

$$\sin(\theta_x) = \frac{k_x}{k}; \sin(\theta_h) = \frac{k_h}{k}; \sin(\theta_e) = \frac{k_e}{k} \quad (13)$$

Intuitively, these various angles are apparent emergence angles as seen on different data gathers. Then the scale function becomes:

$$f = \frac{\sin(\theta_e)}{\sin(\theta_h)} \left( 1 - \frac{\sin^2(\theta_e) - \sin^2(\theta_h)}{1 + \sin^2(\theta_x) - \sin^2(\theta_e)} \right) \quad (14)$$

If we consider an arrival at time  $t$  from a scatterer at  $x_0$ , then these various angles can be approximated as:

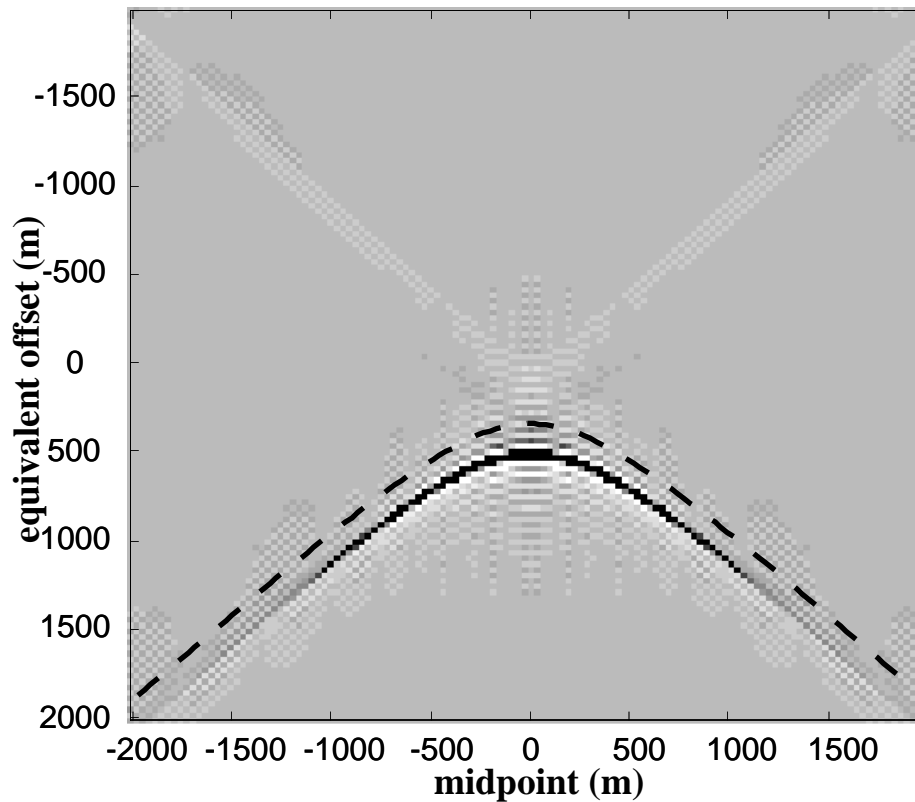


Fig. 7. The result of a numerical simulation of the inverse 2-D Fourier transform of equation (10) is shown. The input data was assumed to be an impulse at  $h = 500$ ,  $x = 0$ , and  $t = 2.0$ . Shown as a gray-level matrix is the  $t = 2.0$  plane of the output in  $(x, h_e)$  space. Shown as a dashed line is the ray theoretic hyperbola from the  $t = 2.0$  plane of figure 4. The ray hyperbola has been shifted up by a constant for clarity and actually overlays the hyperbolic image in the matrix precisely.

$$\sin(\theta_x) = \frac{2(x - x_0)}{vt}; \quad \sin(\theta_h) = \frac{2h}{vt}; \quad \sin(\theta_e) = \frac{2h_e}{vt} \quad (15)$$

When substituted into (14), this allows an approximate evaluation of the scaling function,  $f$ , in the space-time domain.

Equation (9) shows that the CSP gathers are imaged independently to form the migrated section at each  $x$  by a process resembling NMO and stack. In fact, we can consider (9) to be the limiting case of a Stolt-like wavefield in which the equivalent offset, rather than the half-offset, is set to zero. That is, define the "Stolt equivalent" wavefield:

$$\Psi_e(x, h_e, t, z) = \frac{v}{2} \iint \bar{\phi}(x, k_e, k) \exp\left(i \sqrt{k^2 - k_e^2} z\right) \exp\left(-ikvt/2 + ik_e h_e\right) dk_e dk \quad (16)$$

and note that equation (9) results from:

$$\Psi(x, h=0, t=0, z) = \Psi_e(x, h_e=0, t=0, z) \quad (17)$$

The formal similarity between (16) and the post-stack migration equations is striking. In fact, setting  $t = 0$  in (16) gives an identical expression to post-stack Stolt migration for each  $x$ . Thus (16) does indeed say to move energy along hyperbolae in equivalent offset. The imaging operation required for the CSP gathers is thus a 2-D post stack migration, in  $(h_e, t)$  space, with the result being retained only at zero  $h_e$ . As a first order approximation, the gathers can simply be move-out corrected, scaled and stacked. So we conclude:

$$\begin{aligned} \Psi_e(x, h_e, t, z=0) &= \text{the unmigrated CSP gathers} \\ \Psi_e(x, h_e=0, t=0, z) &= \text{the prestack migrated image} \end{aligned}$$

The Fourier theory outlined here is explicitly developed assuming constant velocity; however, an approximate  $v(z)$  extension is easily formulated. First, as has already been noted, the formation of CSP gathers is still valid because a vertical array of scatterers in depth will produce a vertically aligned array of diffraction surfaces in time. Thus the energy which should be imaged at some location  $x$ , is still coherently formed in the CSP gather at that location; so, once formed, the gathers may be imaged independently. Since equivalent wavenumber (and equivalent offset) depend on velocity, their computation must become depth (or vertical travelttime  $t_0$ ) variant. For a Kirchhoff implementation, we have found it satisfactory to regard 'v' in equation (2) as  $v_{rms}(t_0)$ . Of course, the  $v_{rms}$  assumption is only necessary when physical meaning must be ascribed to the imaging velocities. As with conventional stacking, CSP imaging proceeds with the velocities chosen from velocity analysis which best image the CSP gathers. A more complete discussion of velocity analysis of CSP gathers is found in our companion paper (Bancroft et al. 1996).

A Fourier implementation which accommodates vertical velocity variations might proceed with a stretch technique (Stolt 1978, Yilmaz 1987) or with a phase shift method (Gazdag 1978). A cursory examination of the prestack implementation of phase shift migration (Gazdag and Sguazzero, 1984) shows that it will also simplify under the equivalent wavenumber assumption. If the equivalent offset binning is not done, then the process of CSP gather formation is reversible. Hence, with a horizontally layered velocity model, a recursive scheme of forming CSP gathers appropriate for a layer velocity, downward extrapolation through the layer by phase shift, and unforming the gathers is theoretically defensible. As with poststack migration, the result after  $n$  steps will be a phase expression which is a summation of the phase shifts for each step. Also, it seems likely that the phase shift scheme would be highly accurate. However, we have no immediate intention of implementing the Fourier theory, mainly because of the typically irregular prestack geometry, and feel that its main value lies in verifying and improving the Kirchhoff implementation described in Bancroft et al. (1994 and 1996).

The extension to lateral velocity variations seems much more problematic since the CSP gathers are no longer independent. Intuitively, we expect a CSP gather formed at the surface to correspond to scatterpoint locations along an image ray (Hubral and Krey 1980). This suggests that any CSP imaging algorithm which correctly handles lateral velocity variations must allow energy transfer between the gathers. It is not clear that the theory presented here can be extended to this circumstance without major alterations.

## CONCLUSIONS

Prestack time migration may be performed, with high precision and efficiency, by the process of sorting the data into CSP gathers at equivalent offset and then imaging those gathers. This process, called EOM, is the space-time domain Kirchhoff approximation to a Fourier theory, called EWM, which is an exact reformulation of Stolt's (1978) constant velocity algorithm. Both EOM and EWM are based on the recognition that the double square root equations underlying each can be written exactly as single square roots which define equivalent offset and equivalent wavenumber. The EWM process forms the CSP gathers in the Fourier domain by mapping and scaling the 3D spectrum of the 2D prestack wavefield. Imaging of the resultant gathers may be done exactly by an algorithm formally identical to post stack migration of each and retaining only zero equivalent offset or approximately by NMO removal and stacking. The approximate extension of the constant velocity theory to vertical velocity variations is straight forward.

## ACKNOWLEDGMENTS

We wish to thank the sponsors of the CREWES project and Lithoprobe for their support of this research.

## REFERENCES

- Bancroft, J.C. and Geiger, H.D., 1994, Equivalent offsets and CRP gathers for prestack migration: Expanded Abstracts 1994 SEG International Convention, 672-675
- Bancroft, J.C., Wang, S., Foltinek, D.S., and Geiger, H.D., 1995, Common scatter point (CSP) prestack migration: Expanded Abstracts CSEG 1995 National Convention
- Bancroft, J.C., Geiger, H.D., Margrave, G.F., Wang, S., and Foltinek, D.S., 1996, Prestack migration by equivalent offsets and CSP gathers: submitted to Geophysics
- Claerbout, 1985, *Imaging the Earth's Interior*, Blackwell Scientific Publications
- Gazdag, J., 1978, Wave-equation migration by phase shift, *Geophysics*, 43, 1342-1351
- Gazdag, J., and Sguazzero, P., 1984, Migration of Seismic Data, *Proceedings of the IEEE*, 72, 1302-1315
- Hale, I.D., 1983, Dip Moveout by Fourier Transform, Ph.D. thesis, Stanford University
- Hale, D., and Artley, C., 1993, Squeezing dip moveout for depth-variable velocity, *Geophysics*, 58, 257-264
- Hubral, P., and Krey, T., 1980, Interval Velocities from Seismic Reflection Time Measurements, Society of Exploration Geophysicists
- Stolt, R.H., 1978, Migration by Fourier Transform, *Geophysics*, 43, 23-48
- Schneider, W., 1978, Integral formulation for migration in two and three dimensions, *Geophysics*, 43, 49-76
- Yilmaz, O., 1987, *Seismic Data Processing*, Society of Exploration Geophysicists

## APPENDIX A: GENERALIZED EQUIVALENT SQUARE ROOT

In the prestack imaging theory presented in this paper, it is desirable to write the sum of two square roots as a single equivalent square root. We now derive a generalized expression for such an algebraic transformation. The following equation expresses the basic problem:

$$\sqrt{d^2 + a^2} + \sqrt{d^2 + b^2} = 2\sqrt{d^2 + c^2} \quad (\text{A-1})$$

where  $d$ ,  $a$ , and  $b$  are known and  $c$  is to be found in terms of them. Subtracting  $\sqrt{d^2 + b^2}$  from both sides and squaring gives:

$$d^2 + a^2 = 4[d^2 + c^2] + d^2 + b^2 - 4\sqrt{d^2 + b^2}\sqrt{d^2 + c^2} \quad (\text{A-2})$$

Canceling common terms, dividing by  $\sqrt{d^2 + c^2}$ , and rearranging:

$$4\sqrt{d^2 + b^2} = \frac{4[d^2 + c^2] + b^2 - a^2}{\sqrt{d^2 + c^2}} \quad (\text{A-3})$$

squaring:

$$16[d^2 + b^2] = 16[d^2 + c^2] + 8[b^2 - a^2] + \frac{[b^2 - a^2]^2}{d^2 + c^2} \quad (\text{A-4})$$

Rearranging again:

$$c^2 = \frac{1}{2}[a^2 + b^2] - \frac{1}{16} \frac{[a^2 - b^2]^2}{d^2 + c^2} \quad (\text{A-5})$$

This result, though not fully solved for  $c$ , is a good starting point for specialization to specific cases. We note that the denominator of the second term is proportional to the square of equation (A-1), so that formally, it is trivially easy to fully solve for  $c$  by substitution of (A-1) into (A-5). Let us now examine several special cases and verify that this is the correct result.

### Case 1: 2-D Prestack Kirchhoff Imaging

Here the double square root equation of interest is equation (1):

$$vt = \sqrt{z^2 + (x+h)^2} + \sqrt{z^2 + (x-h)^2} = 2\sqrt{z^2 + h_e^2} \quad (\text{A-6})$$

To apply (A-5), let:

$$\begin{aligned} a &= x+h \Rightarrow a^2 = x^2 + 2xh + h^2 \\ b &= x-h \Rightarrow b^2 = x^2 - 2xh + h^2 \\ c &= h_e \text{ and } d = z \end{aligned} \quad (\text{A-7})$$

so, substituting A-7 into A-5 and simplifying gives:

$$h_e^2 = x^2 + h^2 - \frac{4x^2h^2}{v^2t^2} \quad (A-8)$$

This is equation (2). Note that the simplification process used:

$$v^2t^2 = 4(z^2 + h_e^2) \quad (A-9)$$

Also of interest is A-8 solved for h:

$$h^2 = \frac{h_e^2 - x^2}{1 - \frac{4x^2}{v^2t^2}} = \frac{v^2t^2[h_e^2 - x^2]}{v^2t^2 - 4x^2} = \frac{[z^2 + h_e^2][h_e^2 - x^2]}{z^2 + h_e^2 - x^2} \quad (A-10)$$

### Case 2: 2-D Equivalent Wavenumber Imaging

In this case, we wish to solve equation (7) where the square roots we are working with all have a minus sign in them instead of a plus sign. As a starting point we take:

$$\sqrt{k^2 - [k_x + k_h]^2} + \sqrt{k^2 - [k_x - k_h]^2} = 2\sqrt{k^2 - k_e^2} \quad (A-11)$$

If we define:  $a^2 = -A^2$ ,  $b^2 = -B^2$ , and  $c^2 = -C^2$ , then, equation (A-5) becomes:

$$C^2 = \frac{1}{2}[A^2 + B^2] + \frac{1}{16} \frac{[A^2 - B^2]^2}{d^2 - C^2} \quad (A-12)$$

Now, let:

$$\begin{aligned} A &= k_x + k_h \Rightarrow A^2 = k_x^2 + 2k_xk_h + k_h^2 \\ B &= k_x - k_h \Rightarrow B^2 = k_x^2 - 2k_xk_h + k_h^2 \\ C &= k_e \text{ and } d = k \end{aligned} \quad (A-13)$$

and note:

$$k_z^2 = k^2 - k_e^2 \quad (A-15)$$

Substituting (A-14) and (A-15) into (A-13) and simplifying gives:

$$k_e^2 = k_x^2 + k_h^2 + \frac{k_x^2k_h^2}{k_z^2} \quad (A-16)$$

This is the first form for  $k_e$  given in equation 8. To obtain the other, we first substitute (A-14) into (A-15) and solve for  $k_x(k_e, k_h)$  or  $k_h(k_e, k_x)$ :

$$k_x^2 = \frac{k_e^2 - k_h^2}{1 + \frac{k_h^2}{k^2 - k_e^2}} = \frac{[k^2 - k_e^2][k_e^2 - k_h^2]}{k^2 - k_e^2 + k_h^2} \quad (A-16)$$

and

$$k_h^2 = \frac{k_e^2 - k_x^2}{1 + \frac{k_x^2}{k^2 - k_e^2}} = \frac{[k^2 - k_e^2][k_e^2 - k_x^2]}{k^2 - k_e^2 + k_x^2} \quad (\text{A-17})$$

Either of these expressions can be manipulated to obtain a polynomial in  $k_e^2$ :

$$k_e^4 - k_e^2[k_x^2 + k_h^2 + k^2] + k^2 k_x^2 + k_h^2 k_x^2 + k^2 k_h^2 = 0 \quad (\text{A-18})$$

This can be solved for  $k_e^2$  using the quadratic equation. The result is:

$$k_e^2 = \frac{1}{2}[k_x^2 + k_h^2 + k^2] - \frac{1}{2}\sqrt{[k^2 - k_x^2 - k_h^2]^2 - 4k_h^2 k_x^2} \quad (\text{A-19})$$

This is the second form of equation (8). Note that a sign choice has been made for the radical in (A-19). The choice is determined by requiring that  $k_e^2 = k_x^2$  in the limit as  $k_h^2$  approaches zero.

In appendix B, an expression for  $\partial k_h / \partial k_e$  will be required. The easiest way to obtain this is to differentiate (A-18). For example, we differentiate with respect to  $k_e$  with  $k_x$  held constant to find  $\partial k_h / \partial k_e$ . The resultant expression is:

$$\frac{\partial k_h}{\partial k_e} = \frac{k_e}{k_h} [1 - \nu] \quad (\text{A-20})$$

where

$$\nu = \frac{k_e^2 - k_h^2}{k^2 + k_x^2 - k_e^2} = \frac{k_e^2 - k_h^2}{k_z^2 + k_x^2} = \frac{k_x^2 [k_z^2 + k_h^2]}{k_z^2 [k_z^2 + k_x^2]} \quad (\text{A-21})$$

As is evident,  $\nu$  must always be non-negative for real wavenumbers. A similar expression for  $\partial k_x / \partial k_e$  is:

$$\frac{\partial k_x}{\partial k_e} = \frac{k_e}{k_x} [1 - \mu] \quad (\text{A-22})$$

where:

$$\mu = \frac{k_e^2 - k_x^2}{k^2 + k_h^2 - k_e^2} = \frac{k_e^2 - k_x^2}{k_z^2 + k_h^2} = \frac{k_h^2 [k_z^2 + k_x^2]}{k_z^2 [k_z^2 + k_h^2]} \quad (\text{A-23})$$

## APPENDIX B: EQUIVALENT WAVENUMBER MIGRATION DERIVATION

In this appendix, equations (9), (10), (11), and (12) will be derived. The procedure is a straight forward change of integration variables from  $k_h$  to  $k_e$  in (6b) which is the expression for the prestack migrated wavefield:

$$\Psi(x, h=0, t=0, z) = \frac{v}{2} \iiint \phi_0(k_x, k_h, k) \exp(i k_z z) \exp(i k_x x) dk_x dk_h dk \quad (B-1)$$

where  $k=2\omega/v$  has been used. Formally changing variables from  $k_h$  to  $k_e$ :

$$\Psi(x, h=0, t=0, z) = \frac{v}{2} \iiint \phi_0(k_x, k_h(k_e), k) \exp(i k_z z) \exp(i k_x x) dk_x dk \frac{\partial k_h}{\partial k_e} dk_e \quad (B-2)$$

with  $k_h(k_e)$  given by the square root of (A-17). (As with all integrations in this paper, the integration limits are assumed to be over all possible values. Generally this is from  $-\infty$  to  $+\infty$  though care must be taken to ensure that evanescent contributions (i.e. imaginary wavenumbers) result in integration kernels which exponentially decay.) Next we define  $\bar{\phi}_0(k_x, k_e, k)$  which is the result of mapping  $\phi_0(k_x, k_h, k)$  from  $(k_x, k_h, k)$  space to  $(k_x, k_e, k)$  space using equation (A-19):

$$\begin{aligned} \bar{\phi}_0(k_x, k_e, k) &= \bar{\phi}_0\left(k_x, \text{sign}(k_h) \sqrt{\frac{1}{2}[k_x^2 + k_h^2 + k^2]} - \frac{1}{2} \sqrt{[k^2 - k_x^2 - k_h^2]^2 - 4k_h^2 k_x^2}, k\right) \\ &= \phi_0(k_x, k_h, k) \end{aligned} \quad (B-3)$$

This is equation (11). Since equation (8) is a relation between the squares of  $k_h$  and  $k_e$ , it leaves the sign indeterminate and we have chosen to map  $+k_h$  to  $+k_e$  and  $-k_h$  to  $-k_e$ . As depicted in figure 5, contours of constant  $k_e$  (which are also constant  $k_z$  contours) in  $(k_x, k_h)$  space can be seen to grade from nearly circular (near the origin) to nearly diamond shaped (near the evanescent boundary). The spectral mapping takes the upper half of each contour in  $(k_x, k_h)$  space to a horizontal line in the upper triangular region of  $(k_x, k_e)$  space and vice-versa for the lower half of each contour.

Next, substitution of (A-20) and (B-3) into (B-2) results in:

$$\begin{aligned} \Psi(x, h=0, t=0, z) &= \\ \frac{v}{2} \iiint \frac{k_e}{k_h(k_e)} [1 - v(k_x, k_e, k)] \bar{\phi}_0(k_x, k_e, k) \exp(i \sqrt{k^2 - k_e^2} z) \exp(i k_x x) dk_x dk_e dk \end{aligned} \quad (B-4)$$

Note that we have also written  $k_z$  explicitly in terms of  $k$  and  $k_e$ . Since the migration phase shift,  $\exp(ik_z z)$ , no longer contains explicit  $k_x$  dependence, the  $k_x$  integration is a non-phase shifting simple inverse Fourier transform and can be performed first. We define:

$$\bar{\phi}(x, k_e, k) \equiv \int f(k_x, k_e, k) \bar{\phi}_0(k_x, k_e, k) \exp(i k_x x) dk_x \quad (\text{B-5})$$

where:

$$f(k_x, k_e, k) = \frac{k_e}{k_h(k_e)} \left[ 1 - v(k_x, k_e, k) \right] = \frac{k_e}{k_h(k_e)} \left[ 1 - \frac{k_e^2 - k_h^2(k_e)}{k^2 + k_x^2 - k_e^2} \right] \quad (\text{B-6})$$

These are equations (10) and (12). With these definitions, (B-4) becomes:

$$\Psi(x, h=0, t=0, z) = \frac{v}{2} \iint \bar{\phi}(x, k_e, k) \exp\left(i \sqrt{k^2 - k_e^2} z\right) dk_e dk \quad (\text{B-7})$$

This is equation (9).